Properties of the strange axial mesons in the relativized quark model

Harry G. Blundell, Stephen Godfrey,* and Brian Phelps
Ottawa-Carleton Institute for Physics, Department of Physics, Carleton University, Ottawa, Canada K1S 5B6
(Received 6 October 1995)

We study properties of the strange axial mesons in the relativized quark model. We calculate the K_1 decay constant in the quark model and show how it can be used to extract the $K_1(^3P_1)-K_1(^1P_1)$ mixing angle (θ_K) from the weak decay $\tau\to K_1\nu_\tau$. The ratio $B(\tau\to\nu_\tau K_1(1270))/B(\tau\to\nu_\tau K_1(1400))$ is the most sensitive measurement and also the most reliable since the largest of the theoretical uncertainties factor out. However, the current bounds extracted from the TPC/Two-Gamma Collaboration measurements are rather weak: we typically obtain $-30°\lesssim\theta_K\lesssim 50°$ at 68% C.L. We also calculate the strong OZI-allowed decays in the pseudoscalar emission model and the flux-tube-breaking model and extract a $^3P_1$-$^1P_1$ mixing angle of $\theta_K\simeq 45°$. Our analysis also indicates that the heavy quark limit does not give a good description of the strange mesons.

PACS number(s): 13.25.Jx, 12.39.Jh, 12.39.Ki, 12.39.Pn

I. INTRODUCTION

The strange axial mesons offer interesting possibilities for the study of QCD in the nonperturbative regime through the mixing of the $^3P_1$ and $^1P_1$ states. In the SU(3) limit these states do not mix, just as the a_1 and b_1 mesons do not mix. For a strange quark mass greater than the up and down quark masses, SU(3) is broken so that the $^3P_1$ and $^1P_1$ states mix to give the physical K_1 states. In the heavy quark limit, where the strange quark becomes infinitely heavy, the light quark's spin couples with the orbital angular momentum resulting in the light quark having total angular momentum $j=\frac{2}{3}$ in one state and $j=\frac{1}{2}$ in the other state, each state having distinct properties [1–3]. By studying the strange axial mesons and comparing them to the heavy quark limit, one might gain some insights about hadronic properties in the *soft* QCD regime.

Recently, the TPC/Two-Gamma Collaboration has presented measurements for the decays $\tau^-\to\nu_\tau K_1^-(1270)$ and $\tau^-\to\nu_\tau K_1^-(1400)$ [4]. It is expected that the LEP, CLEO, and BES Collaborations, with their large samples of τ's, will be able to study these decays in further detail [5]. These decays provide another means of studying $^3P_1$-$^1P_1$ mixing of the strange axial mesons in addition to using their partial decay widths and masses.

In this paper we study the properties of the strange axial mesons in the context of the relativized quark model [6,7]. We compare the experimental measurements to the predictions of the model to extract the $^3P_1$-$^1P_1$ mixing angle (θ_K). Comparing both the experimental measurements and model results to various limits helps in understanding the nature of QCD in the *soft* regime.

We begin in Sec. II with a brief description of the relativized quark model and a description of the $^3P_1$-$^1P_1$ mixing. By comparing the mass predictions of the quark model to the observed K_1 masses we obtain our first estimate for θ_K. In Sec. III we calculate the K_1 decay constants using the mock-meson approach and use the results to obtain a second estimate of θ_K. In Sec. IV we study the strong decay properties of these states using the pseudoscalar emission model [6] and the flux-tube-breaking model [8] and use the results as another way of measuring the $^3P_1$-$^1P_1$ mixing angle. When appropriate, we examine the nonrelativistic and heavy quark limits to gain insights into the underlying dynamics. Various aspects of the phenomenology of the strange axial mesons have also been studied by Suzuki in a series of recent papers [9,10], using approaches complementary to ours.

II. THE K_1 MASSES AND $^3P_1-^1P_1$ MIXING

In this section we give a very brief description of the relativized quark model [6,7]. The spin-orbit contributions, in particular, will be important in understanding the $^3P_1$-$^1P_1$ mixing. The model is not derived from first principles but is rather motivated by expected relativistic properties. Although progress is being made using more rigorous approaches, the relativized quark model describes the properties of hadrons reasonably well and presents an approach which can give insights into the underlying dynamics that can be obscured in the more rigorous approaches.

The basic equation of the model is the rest frame Schrödinger-type equation. The effective potential, $V_{q\bar{q}}(\vec{p},\vec{r})$, is described by a Lorentz-vector one-gluon-exchange interaction at short distances and a Lorentz-scalar linear confining interaction. $V_{q\bar{q}}(\vec{p},\vec{r})$ was found by equating the scattering amplitude of free quarks, using a scattering kernel with the desired Dirac structure, with the effects between bound quarks inside a hadron [11]. Because of the relativistic effects, the potential is momentum dependent in addition to being coordinate dependent. The details of the model can be found in Ref. [6]. To first order in $(v/c)^2$, $V_{q\bar{q}}(\vec{p},\vec{r})$ reduces to the standard nonrelativistic result

$$V_{q\bar{q}}(\vec{p},\vec{r})\to V(\vec{r})=H_{q\bar{q}}^{\rm conf}+H_{q\bar{q}}^{\rm cont}+H_{q\bar{q}}^{\rm ten}+H_{q\bar{q}}^{\rm SO}, \qquad (1)$$

where

$$H_{q\bar{q}}^{\rm conf}=C+br+\frac{\alpha_s(r)}{r}\vec{F}_q\cdot\vec{F}_{\bar{q}} \qquad (2)$$

*Electronic address: godfrey@physics.carleton.ca

includes the spin-independent linear confinement and Coulomb-like interaction,

$$H_{q\bar{q}}^{\rm cont}=-\frac{8\pi}{3}\frac{\alpha_s(r)}{m_q m_{\bar{q}}}\vec{S}_q\cdot\vec{S}_{\bar{q}}\delta^3(\vec{r})\vec{F}_q\cdot\vec{F}_{\bar{q}} \tag{3}$$

is the color contact interaction,

$$H_{q\bar{q}}^{\rm ten}=-\frac{\alpha_s(r)}{m_q m_{\bar{q}}}\frac{1}{r^3}\left[\frac{3\vec{S}_q\cdot\vec{r}\vec{S}_{\bar{q}}\cdot\vec{r}}{r^2}-\vec{S}_q\cdot\vec{S}_{\bar{q}}\right]\vec{F}_q\cdot\vec{F}_{\bar{q}} \tag{4}$$

is the color tensor interaction,

$$H_{q\bar{q}}^{\rm SO}=H_{q\bar{q}}^{\rm SO(CM)}+H_{q\bar{q}}^{\rm SO(TP)} \tag{5}$$

is the spin-orbit interaction with

$$H_{q\bar{q}}^{\rm SO(CM)}=-\frac{\alpha_s(r)}{r^3}\left(\frac{\vec{S}_q}{m_q m_{\bar{q}}}+\frac{\vec{S}_{\bar{q}}}{m_q m_{\bar{q}}}+\frac{\vec{S}_q}{m_q^2}+\frac{\vec{S}_{\bar{q}}}{m_{\bar{q}}^2}\right)\cdot\vec{L}\vec{F}_q\cdot\vec{F}_{\bar{q}} \tag{6}$$

its color magnetic piece arising from one-gluon exchange and

$$H_{q\bar{q}}^{\rm SO(TP)}=-\frac{1}{2r}\frac{\partial H_{q\bar{q}}^{\rm conf}}{\partial r}\left(\frac{\vec{S}_q}{m_q^2}+\frac{\vec{S}_{\bar{q}}}{m_{\bar{q}}^2}\right)\cdot\vec{L} \tag{7}$$

the Thomas precession term. In these formulas, $\langle\vec{F}_q\cdot\vec{F}_{\bar{q}}\rangle=-4/3$ for a meson and $\alpha_s(r)$ is the running coupling constant of QCD.

For the case of a quark and antiquark of unequal mass, the $^3P_1$ and $^1P_1$ states can mix via the spin-orbit interaction or some other mechanism. Consequently, the physical $j=1$ states are linear combinations of $^3P_1$ and $^1P_1$ which we describe by the mixing

$$\begin{aligned}K_{1(\rm low)}^+&=(^1P_1)^+\cos\theta+(^3P_1)^+\sin\theta=K_b^+\cos\theta+K_a^+\sin\theta,\\ K_{1(\rm high)}^+&=-(^1P_1)^+\sin\theta+(^3P_1)^+\cos\theta\\&=-K_b^+\sin\theta+K_a^+\cos\theta.\end{aligned} \tag{8}$$

The Hamiltonian problem was solved using the following parameters: the slope of the linear confining potential is 0.18 $\rm GeV^2$, $m_u=m_d=0.22$ GeV, and $m_s=0.419$ GeV. The resulting masses of the unmixed states are

$$M(K_a)=1.37\ \text{GeV},\quad M(K_b)=1.35\ \text{GeV}. \tag{9}$$

We expect these values to be reasonable estimates as the model's predictions for the closely related a_1 and b_1 masses are consistent with the experimental measurements. In this model spin-orbit mixing results in $\theta_K=-5°$ [3] but the K_1 masses remain the same within the given numerical precision. These mixed masses and the mixing angle are not consistent with the measured values.

We can obtain a phenomenological estimate of θ_K by considering the 2×2 matrix relating K_a and K_b to the physical K_1's. We do not make any assumptions about the origin of the $^3P_1$-$^1P_1$ mixing and treat the off-diagonal matrix element of the K_1 mass matrix as a free parameter. Diagonalizing the K_a-K_b mass matrix gives the relation between θ_K and the mass differences:

$$\cos2\theta_K=\frac{M(K_a)-M(K_b)}{M(K_1(1402))-M(K_1(1273))} \tag{10}$$

with corresponding K_1 masses

$$\begin{aligned}M_{\rm low}&=M_b\cos^2\theta_K+M_a\sin^2\theta_K-(M_a-M_b)\frac{\sin^2 2\theta_K}{2\cos2\theta_K},\\ M_{\rm high}&=M_b\sin^2\theta_K+M_a\cos^2\theta_K+(M_a-M_b)\frac{\sin^2 2\theta_K}{2\cos2\theta_K}.\end{aligned} \tag{11}$$

Solving gives $\theta_K\simeq\pm41°$. Note that degenerate K_a and K_b masses will always result in a mixing angle of $\pm45°$ [12]. Thus, the value we obtain for θ_K is more a reflection of the near degeneracy of the model's prediction for M_{K_a} and M_{K_b} than anything else and one should not read too much into the value we extract here.

III. WEAK COUPLINGS OF THE K_1's

We use the mock-meson approach to calculate the hadronic matrix elements [6,13–17]. The basic assumption of the mock-meson approach is that physical hadronic amplitudes can be identified with the corresponding quark model amplitudes in the weak binding limit of the valence quark approximation. This correspondence is exact only in the limit of zero binding and in the hadron rest frame. Away from this limit, the amplitudes are not, in general, Lorentz invariant by terms of order p_i^2/m_i^2. In this approach the mock meson, which we denote by $\tilde{M}$, is defined as a state of a free quark and antiquark with the wave function of the physical meson, M:

$$\begin{aligned}|\tilde{M}(\vec{K})\rangle=\sqrt{2M_{\tilde{M}}}\int d^3p\ \Phi_M(\vec{p})\chi_{s\bar{s}}\phi_{q\bar{q}}\phi_{\rm color}\\ \times|q[(m_q/\mu)\vec{K}+\vec{p},s]\bar{q}[(m_{\bar{q}}/\mu)\vec{K}-\vec{p},\bar{s}]\rangle,\end{aligned} \tag{12}$$

where $\Phi_M(\vec{p})$, $\chi_{s\bar{s}}$, $\phi_{q\bar{q}}$, and $\phi_{\rm color}$ are momentum, spin, flavor, and color wave functions, respectively, $\mu=m_q+m_{\bar{q}}$, $\vec{K}$ is the mock-meson momentum, $M_{\tilde{M}}$ is the mock-meson mass, and $\sqrt{2M_{\tilde{M}}}$ is included to normalize the mock-meson wave function. To calculate the hadronic amplitude, the physical matrix element is expressed in terms of Lorentz covariants with Lorentz-scalar coefficients A. In the simple cases when the mock-meson matrix element has the same form as the physical meson amplitude, we simply take $A=\tilde{A}$.

In the case of interest, the axial meson decay constants are expressed as:

$$\langle0|\bar{q}\gamma^\mu(1-\gamma_5)q|M(\vec{K},\lambda)\rangle=\frac{i}{(2\pi)^{3/2}}f_{K_1}\epsilon^\mu(\vec{K},\lambda), \tag{13}$$

where $\epsilon^\mu(\vec{K},\lambda)$ is the K_1 polarization vector and f_{K_1} is the appropriate K_1 decay constant. To calculate the left-hand side of Eq. (13), we first calculate

$$\langle 0|\bar{q}\gamma^\mu(1-\gamma_5)q|q[(m_q/\mu)\vec{K}+\vec{p},s]\bar{q}[(m_{\bar{q}}/\mu)\vec{K}-\vec{p},\bar{s}]\rangle, \tag{14}$$

using free quark and antiquark wave functions and weight the result with the meson's momentum space wave function.

There are a number of ambiguities in the mock-meson approach and different prescriptions have appeared in the literature. For example, there are several different definitions for the mock-meson mass ($M_{\tilde{M}}$) appearing in Eq. (12). To be consistent with the mock-meson prescription, we should use the mock-meson mass defined as $\langle E_q\rangle+\langle E_{\bar{q}}\rangle$. However, because it is introduced to give the correct relativistic normalization of the meson's wave function, the physical mass is another, perhaps more appropriate, definition. The second ambiguity is the question of which component of the four-vector in Eq. (13) we should use to obtain f_{K_1}. In principle, it should not matter as both the left- and right-hand sides of Eq. (13) are Lorentz four-vectors. This is true in the weak binding limit where binding effects are totally neglected, but in practice, this is not the case. We follow Ref. [13] and extract f_{K_1} using the spatial components of Eq. (13) in the limit $\vec{K}\to 0$. Finally, evaluating Eq. (14) introduces factors of $\sim m_i/E_i$. While some prescriptions take the expression derived from Eq. (13) only as a guideline and introduce powers of $\sim(m_i/E_i)^\epsilon$ with ϵ an arbitrary power, we chose to use the expression exactly as derived from Eq. (13). The different prescriptions are described in greater detail in Ref. [13] which calculated the pseudoscalar decay constants (f_K). We will follow the approach taken there and use the variations in prescriptions as a measure of how seriously we should take our results. In our results we, therefore, use the ''exact'' expression for f_{K_1} and we take $M_{\tilde{M}}$ to be equal to the physical mass ($M_{\rm phys}$). Variations in the mock-meson normalization result in variations in f_{K_1} of at most 20%. Results using the physical mass lie in the middle of the range so that we expect uncertainties introduced by taking $M_{\tilde{M}}\equiv M_{\rm phys}$ to be no more than $\sim$10%. As in Ref. [13], f_{K_1} was most sensitive to the wave function used. Here, we use the sets of wave functions that gave the best agreement with experiment for f_K in Ref. [13]. We choose two possibilities, one which underestimated f_K and one which overestimated it. We would expect these choices to likewise bound the actual value of the f_{K_1}.

The expressions we obtain for f_{K_1} are given by

$$f_{K_1}(^3P_1)=-\frac{4\sqrt{3}}{3}\sqrt{M_{\tilde{K}_1}}\int\frac{d^3p}{(2\pi)^{3/2}}\left(i\sqrt{\frac{3}{8\pi}}\phi_{K_1}(p)\right)\times p\left[\left(\frac{E_q+m_q}{2E_q}\right)\left(\frac{E_{\bar{q}}+m_{\bar{q}}}{2E_{\bar{q}}}\right)\right]^{1/2}\times\left[\frac{1}{E_q+m_q}+\frac{1}{E_{\bar{q}}+m_{\bar{q}}}\right],$$

$$f_{K_1}(^1P_1)=+\frac{2\sqrt{6}}{3}\sqrt{M_{\tilde{K}_1}}\int\frac{d^3p}{(2\pi)^{3/2}}\left(i\sqrt{\frac{3}{8\pi}}\phi_{K_1}(p)\right)\times p\left[\left(\frac{E_q+m_q}{2E_q}\right)\left(\frac{E_{\bar{q}}+m_{\bar{q}}}{2E_{\bar{q}}}\right)\right]^{1/2}\times\left[\frac{1}{E_q+m_q}-\frac{1}{E_{\bar{q}}+m_{\bar{q}}}\right], \tag{15}$$

where $\phi_{K_1}(p)$ is the radial part of the momentum space wave function, $E_q=\sqrt{|\vec{p}|^2+m_q^2}$ and $E_{\bar{q}}=\sqrt{|\vec{p}|^2+m_{\bar{q}}^2}$. In the SU(3) limit, only K_a couples to the weak current.

With the definition of f_{K_1} given by Eq. (13), the partial width for $\tau\to K_1\nu_\tau$ is given by

$$\Gamma(\tau\to K_1\nu_\tau)=\frac{G_F^2|V_{us}|^2f_{K_1}^2m_\tau^3}{16\pi m_{K_1}^2}(1-m_{K_1}^2/m_\tau^2)^2\times(1+2m_{K_1}^2/m_\tau^2). \tag{16}$$

A. The nonrelativistic limit

It is useful to examine the K_1 decay constants in the nonrelativistic limit, where their qualitative properties are more transparent. In this limit, the axial-vector meson decay constants become

$$f_{K_1}(^3P_1)=-\sqrt{12M_{\widetilde{K_1}}}\left[\frac{1}{m_q}+\frac{1}{m_{\bar{q}}}\right]\sqrt{\frac{3}{8\pi}}\frac{\partial R_P(r)}{\partial r}\bigg|_{r=0},$$

$$f_{K_1}(^1P_1)=\sqrt{6M_{\widetilde{K_1}}}\left[\frac{1}{m_q}-\frac{1}{m_{\bar{q}}}\right]\sqrt{\frac{3}{8\pi}}\frac{\partial R_P(r)}{\partial r}\bigg|_{r=0}, \tag{17}$$

where $R_P(r)$ is the radial part of the coordinate space wave function. Combining the weak decay amplitudes with the mixed K_1 eigenstates, the decay constants for the mixed $|K^+\rangle=-|u\bar{s}\rangle$ states are given by[1]

$$f_{K_{\rm low}}=-A\left[\left(\frac{1}{m_u}-\frac{1}{m_s}\right)\cos\theta_K-\sqrt{2}\left(\frac{1}{m_u}+\frac{1}{m_s}\right)\sin\theta_K\right],$$

$$f_{K_{\rm high}}=+A\left[\left(\frac{1}{m_u}-\frac{1}{m_s}\right)\sin\theta_K+\sqrt{2}\left(\frac{1}{m_u}+\frac{1}{m_s}\right)\cos\theta_K\right], \tag{18}$$

where we have defined

$$A=\sqrt{6M_{\widetilde{K_1}}}\left(\sqrt{\frac{3}{8\pi}}\frac{\partial R_P(r)}{\partial r}\bigg|_{r=0}\right). \tag{19}$$

In the SU(3) limit, $f_{K_1}(^1P_1)$ explicitly goes to zero and only the $^3P_1$ state couples to the weak current. The K_b coupling therefore goes like the SU(3) breaking (m_s-m_d).

[1]Note that the sign change going from Eq. (17) to Eq. (18) comes from the phase in the K^+ flavor wave function.

TABLE I. Axial-vector decay constants in the nonrelativistic limit using simple harmonic oscillator wave functions. The f_{K_1} for $|K^+\rangle = -|u\bar{s}\rangle$ are given in units of GeV^2.

Parameter set	$M_{K_1}=1.273$ GeV	$M_{K_1}=1.402$ GeV
Set 1[a]	$f_{K_b}=-0.049$	$f_{K_b}=-0.050$
	$f_{K_a}=+0.269$	$f_{K_a}=+0.283$
Set 2[b]	$f_{K_b}=-0.070$	$f_{K_b}=-0.073$
	$f_{K_a}=+0.396$	$f_{K_a}=+0.415$

[a]From Ref. [18] with $\beta=0.257$ GeV, $m_u=m_d=0.33$ GeV, and $m_s=0.55$ GeV.
[b]From Ref. [17] with $\beta=0.3$ and $m_u=m_d$ and m_s as above.

B. Extracting θ_K using the nonrelativistic expressions

We can obtain an estimate of the $^3P_1$-$^1P_1$ mixing angle by comparing the quark model predictions to experiment. As stated above, the values of the decay constants were quite sensitive to the choice of wave function. We calculated the f_{K_1} for two sets of wave functions that gave the best agreement between a quark model calculation and experiment for the pseudoscalar decay constants [13]. We expect that the actual values for the f_{K_1} will lie between the values predicted using these wave functions. The values for the two meson masses and two sets of wave functions are given in Table I.

There are four measurements that can be used to constrain θ_K. The TPC/Two-Gamma Collaboration [4] has made the measurements:

$$B(\tau\rightarrow\nu K_1(1270))=(0.41^{+0.41}_{-0.35})\times10^{-2}, \tag{20}$$

$$B(\tau\rightarrow\nu K_1(1400))=(0.76^{+0.40}_{-0.33})\times10^{-2}, \tag{21}$$

$$B(\tau\rightarrow\nu K_1)=(1.17^{+0.41}_{-0.37})\times10^{-2}, \tag{22}$$

and Alemany [19] combines CLEO and ALEPH data [20] to obtain:

$$B(\tau\rightarrow\nu K_1)=(0.77\pm0.12)\times10^{-2}, \tag{23}$$

which is smaller than, but consistent with, the TPC/Two-Gamma result. CLEO claims that the τ decays preferentially to the $K_1(1270)$.

Using the ratio $B(\tau\rightarrow\nu K_1(1270))/B(\tau\rightarrow\nu K_1(1400))$ has the advantage of factoring out the uncertainties associated with the K_1 wave function. The ratio is given by[2]

$$R=1.83\left|\frac{\sin\theta_K-\delta\cos\theta_K}{\cos\theta_K+\delta\sin\theta_K}\right|^2, \tag{24}$$

where 1.83 is a phase space factor and δ is an SU(3)-breaking factor given by

$$\delta=\frac{1}{\sqrt{2}}\left(\frac{m_s-m_u}{m_s+m_u}\right). \tag{25}$$

The ratio R is plotted in Fig. 1(a) as a function of θ_K. Taking $m_u=0.33$ GeV and $m_s=0.55$ GeV and fitting Eq. (24) to the ratio of the TPC/Two-Gamma results, we obtain $-30°\lesssim\theta_K\lesssim50°$ at 68% C.L. where the large uncertainty is directly attributed to the large errors in the branching ratios.[3]

Although the relative errors for the individual branching ratios are smaller than those of the ratio, especially for the sum to the two K_1 states, using the branching ratios introduces additional uncertainties because of the errors associated with the meson wave function. In addition, the branching ratios turn out to be less sensitive to θ_K than the ratio is. This is seen very clearly in Figs. 1(b)–1(d) where we have plotted the branching ratios for $\tau\rightarrow\nu_\tau K_1(1270)$, $\tau\rightarrow\nu_\tau K_1(1400)$ and the sum of the two, respectively. The values $\tau_\tau=(295.6\pm3.1)\times10^{-15}$ s and $|V_{us}|=0.2205\pm0.0018$ were used to obtain these curves [21]. The two curves in each figure represent the two wave functions we use and we have included the experimental value with its error. In Fig. 1(d) both the TPC/Two-Gamma and the CLEO and ALEPH values are shown. It is apparent from these figures that it is not particularly meaningful to extract a value for θ_K from these results and any value would be very model dependent. Clearly, better data are needed. The ratio of the rates into the individual final states will give the most model-independent constraints on θ_K.

C. Extracting θ_K using the relativized expressions

We next calculate the axial meson decay constants using the relativized formula of Eq. (15). One might question the importance of including relativistic corrections. However, we need only consider the importance of another relativistic correction: QCD hyperfine interactions which give rise to the $\rho-\pi$, K^*-K, . . . , B^*-B splittings [22]. Although it is difficult to gauge the importance of relativistic corrections to the f_{K_1}, if nothing else their inclusion acts as one more means of judging the reliability of the results.

As in the previous section, we give results for two wave function sets that give reasonable agreement for the f_K in a similar calculation. The various f_{K_1} are given in Table II. We expect that the actual values will lie between the two values given for each case. The predictions for the various branching fractions are shown in Fig. 2 as functions of θ_K along with the experimental values. The most reliable constraint again comes from the ratio of branching fractions which gives $-35°\lesssim\theta_K\lesssim45°$ at 68% C.L. One could also extract values using $B(\tau\rightarrow\nu K_1(1400))$ and $B(\tau\rightarrow\nu K_1(1270))$ but as in the nonrelativistic case, these values are quite sensitive to the magnitude of f_{K_1} which depends on the poorly known K_1 wave functions.

We conclude that the decays $\tau\rightarrow\nu K_1$ offer a means of measuring the $^3P_1$-$^1P_1$ mixing angle but to do so will require more precise measurements than are currently available.

[2]The numbers from Table I give a slightly different value since the different K_1 masses in our expression for f_{K_1} do not exactly factor out.

[3]The χ^2 of the fit actually has two local minima corresponding to both a negative and a positive solution. However, since the hump separating the two solutions is approximately equal to $\Delta\chi^2\lesssim1$, the entire range given for θ_K is consistent at 68% C.L.

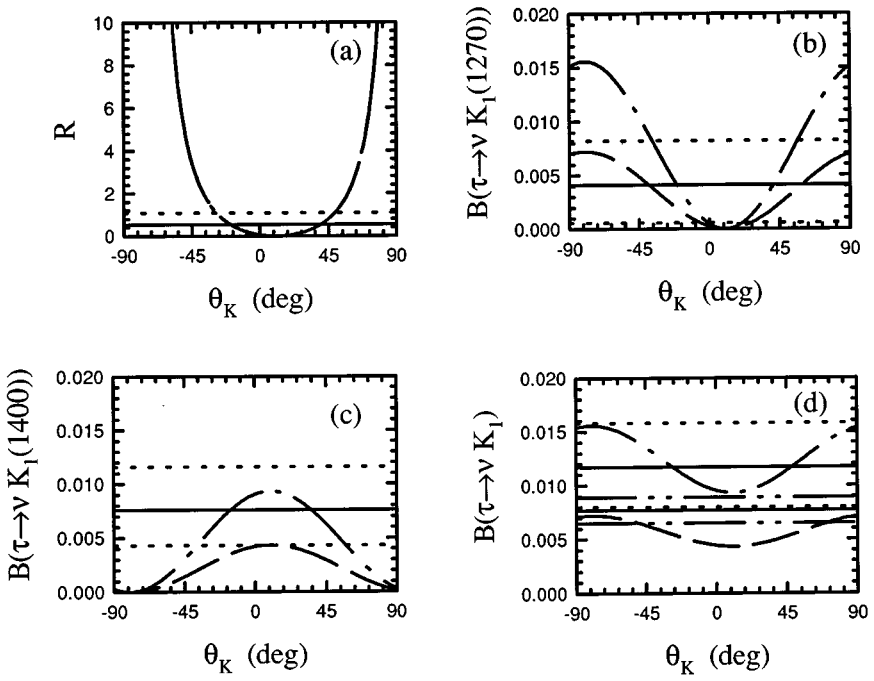

FIG. 1. The $\tau \to K_1 \nu$ decay widths as functions of θ_K for the nonrelativistic results. $R = B(\tau \to \nu K_1(1270))/B(\tau \to \nu K_1(1400))$. In all figures the dashed curve is for the wave functions from Ref. [18] and the dot-dashed curve is for the wave functions from Ref. [17]. In the figure for R, both curves lie on each other. The solid and dotted lines are for the experimental values and their $1-\sigma$ errors from the TPC/Two-Gamma measurement [4]. In addition, in the figure for $B(\tau \to \nu K_1)$, the solid line bounded by the dot-dot-dashed lines are for the CLEO and ALEPH result and their $1-\sigma$ error [19].

IV. STRONG DECAYS OF THE K_1's

It is well known that the strong decays of the K_1 mesons provides a means of extracting the $^3P_1$-$^1P_1$ mixing angle [23]. In particular, the $B(K_1(1270) \to K^*\pi)/B(K_1(1400) \to K^*\pi)$ and $B(K_1(1270) \to K\rho)/B(K_1(1400) \to K\rho)$ ratios have been especially useful. We examine the decays to the final states $K\rho$, $K\omega$, and $K^*\pi$. Although other decays are observed, they lie below threshold and proceed through the tails of the Breit-Wigner resonances making the calculations less reliable. In this section we examine the strong K_1 decays using the pseudoscalar emission model [6], the $^3P_0$ model (also known as the quark-pair creation model) [24], and the flux-tube-breaking model [8]. We concentrate on the decays $K_1 \to K^*\pi$ and $K_1 \to \rho K$.

For the decays $K_1 \to VP$, where V and P denote vector and pseudoscalar mesons, respectively, the Okubo-Zweig-Iizuka (OZI)-rule-allowed decays can be described by two independent S- and D-wave amplitudes which we label S and D. The decay amplitudes, using the conventions of Eq. (8), are given by

$$A(K_1^{\rm low} \to [K^*\pi]_S) = -S\ \sin(\theta_K - \theta_0),$$

$$A(K_1^{\rm low} \to [K^*\pi]_D) = +D\ \cos(\theta_K - \theta_0),$$

$$A(K_1^{\rm high} \to [K^*\pi]_S) = -S\ \cos(\theta_K - \theta_0),$$

$$A(K_1^{\rm high} \to [K^*\pi]_D) = -D\ \sin(\theta_K - \theta_0),$$

$$A(K_1^{\rm low} \to [\rho K]_S) = +S\ \sin(\theta_K + \theta_0),$$

$$A(K_1^{\rm low} \to [\rho K]_D) = +D\ \cos(\theta_K + \theta_0),$$

$$A(K_1^{\rm high} \to [\rho K]_S) = +S\ \cos(\theta_K + \theta_0),$$

$$A(K_1^{\rm high} \to [\rho K]_D) = -D\ \sin(\theta_K + \theta_0),$$

$$A(K_1^{\rm high} \to [\omega K]_S) = +\sqrt{\frac{1}{3}} S\ \cos(\theta_K + \theta_0),$$

$$A(K_1^{\rm high} \to [\omega K]_D) = -\sqrt{\frac{1}{3}} D\ \sin(\theta_K + \theta_0), \qquad (26)$$

where $\sin\theta_0 = \sqrt{1/3}$ and $\cos\theta_0 = \sqrt{2/3}$ and the subscripts S and D refer to S- and D-wave decays. In the heavy quark limit, the $j = 1/2$ state decays into $K^*\pi$ in an S wave and the $j = 3/2$ state decays into $K^*\pi$ in a D wave. Since the decay $K_1(1400) \to K^*\pi$ is dominantly S wave while the decay $K_1(1270) \to K^*\pi$ has comparable S- and D-wave contributions, we conclude that experimental data favors the heavier $J^P = 1^+$ to be mainly $j = 1/2$ and the lighter one to be mainly $j = 3/2$.

TABLE II. Axial-vector decay constants using the relativized mock-meson matrix elements. Simple harmonic oscillator wave functions are used with the parameters given below. The f_{K_1} for $|K^+\rangle = -|u\bar{s}\rangle$ are given in units of GeV^2.

Parameter set	$M_{K_1} = 1.273$ GeV	$M_{K_1} = 1.402$ GeV
Set 1[a]	$f_{K_b} = -0.024$	$f_{K_b} = -0.025$
	$f_{K_a} = +0.220$	$f_{K_a} = +0.231$
Set 2[b]	$f_{K_b} = -0.040$	$f_{K_b} = -0.042$
	$f_{K_a} = +0.486$	$f_{K_a} = +0.510$

[a]From Ref. [17] with $\beta = 0.3$, $m_u = m_d = 0.33$ GeV, and $m_s = 0.55$ GeV.

[b]We used effective oscillator parameters from Ref. [6]. They were obtained by fitting simple harmonic oscillator wave functions to the rms radii of the wave functions of Ref. [6] to obtain $\beta_{K_1} = 0.45$ GeV, $m_u = m_d = 0.22$ GeV, and $m_s = 0.419$ GeV.

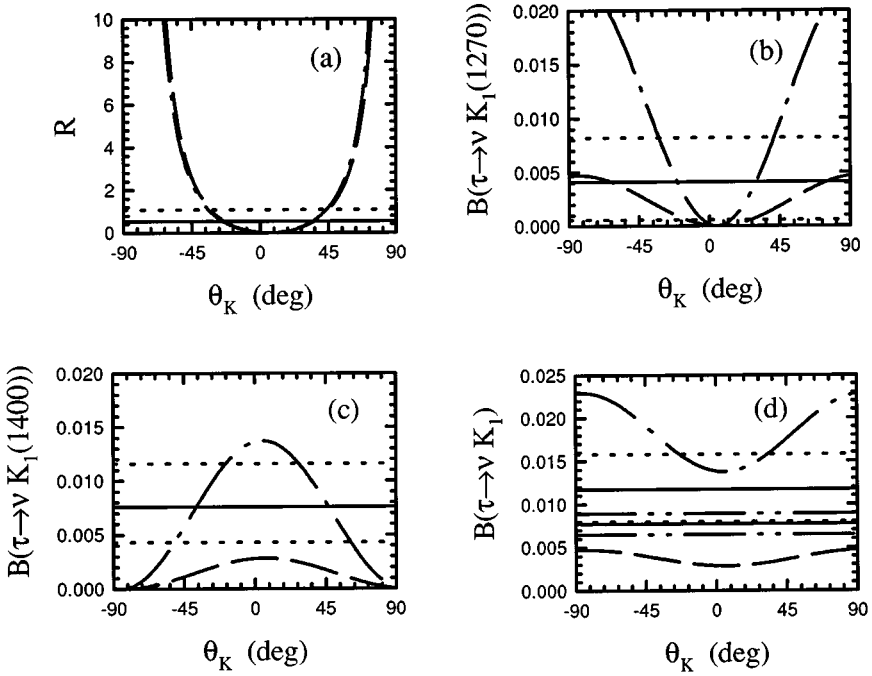

FIG. 2. The $\tau \to K_1 \nu$ decay widths as a function of θ_K for the relativized results. In all figures the dashed curve is for the wave function from Ref. [6] and the dot-dashed curve is for the wave function from Ref. [17]. The other line labeling is the same as in Fig. 1.

In the following subsections we give results for these amplitudes, the resulting decay widths, and the fitted values of θ_K for the various decay models.

A. Decays by the pseudoscalar-meson emission model

In this approach, meson decay proceeds through a single-quark transition via the emission of a pseudoscalar meson [6]. We assume that the pair creation of u, d, and s quarks is approximately SU(3) symmetric. We follow Ref. [6] and use the various approximations introduced there. The resulting amplitudes are given by

$$D = \frac{1}{2} A \tilde{q}^2 F(q^2), \tag{27}$$

$$S = \tilde{S} F(q^2), \tag{28}$$

where $A = 1.67$, $\tilde{S} = 3.27$, q is the momentum of each outgoing meson in the center-of-mass (CM) frame, $\tilde{q} = q/\beta$, $\beta = 0.4$ GeV, and

$$F(q^2) = \sqrt{\frac{1}{2}} \left(\frac{q}{2\pi} \right)^{1/2} \exp(-q^2/(16\beta^2)). \tag{29}$$

Numerical values for the amplitudes are given in Table III.

The partial widths for $K_1 \to K^* \pi$ and $K_1 \to \rho K$ and the ratio of the D to S amplitudes for $K_1 \to K^* \pi$ are plotted in Fig. 3 as functions of θ_K for the $K_1(1270)$ and $K_1(1400)$. The experimental values are given with their errors. From the figures it is clear that the experimental values for $K_1(1270) \to K^* \pi$, $K_1(1400) \to \rho K$, and $A_D/A_S[K_1(1400)]$ correspond to minima in the quark model results with $\theta_K \sim 45°$. We performed a χ^2 fit to the data listed in Table IV and obtained $\theta_K = 48° \pm 5°$. We also allowed the $\tilde{S}$, A, and β parameters to vary and obtained very similar results, the main difference being that the χ^2 value at the minimum decreased significantly. The partial widths and $A_D/A_S(K_1 \to K^* \pi)$ ratios are given in Table IV for the fitted value of θ_K.

B. Decays by the flux-tube breaking model

The flux-tube-breaking model is a variation of the $^3P_0$ model which more closely describes the actual decay processes. In the $^3P_0$ model the elementary process is described by the creation of a $q\bar{q}$ pair with the quantum numbers of the vacuum, $J^{PC} = 0^{++}$. The greatest advantage of this approach is that it requires only one overall normalization constant for the pair creation process. In the flux-tube-breaking model,

TABLE III. Strong decay amplitudes for the strange axial mesons using the pseudoscalar emission model, the $^3P_0$ decay model and the flux-tube-breaking model. Note that the amplitudes include phase space and are all given in units of MeV$^{1/2}$.

		$^3P_0$	Flux-tube breaking	
Amplitude	Pseudoscalar	Set 1[a]	Set 1[a]	Set 2[b]
γ	emission	6.25	10.4	12.8
$S(K_1^{\text{low}} \to \rho K)$	8.02	8.81	8.50	11.0
$D(K_1^{\text{low}} \to \rho K)$	0.074	0.056	0.057	0.055
$S(K_1^{\text{low}} \to K^* \pi)$	15.5	15.5	14.8	20.5
$D(K_1^{\text{low}} \to K^* \pi)$	2.23	2.36	2.43	2.29
$S(K_1^{\text{high}} \to \rho K)$	15.4	15.5	14.8	20.1
$D(K_1^{\text{high}} \to \rho K)$	2.18	2.28	2.34	2.25
$S(K_1^{\text{high}} \to K^* \pi)$	17.3	15.1	14.2	20.7
$D(K_1^{\text{high}} \to K^* \pi)$	4.45	4.61	4.74	4.44
$S(K_1^{\text{high}} \to K \omega)$	15.1	15.4	14.7	20.0
$D(K_1^{\text{high}} \to K \omega)$	1.96	2.04	2.10	2.02

[a]Simple harmonic oscillator wave functions with $\beta = 0.40$ GeV, $m_u = 0.33$ GeV, and $m_s = 0.55$ GeV.
[b]Wave functions from Ref. [6].

the flux-tube-like structure of the decaying meson and its implications for $^3P_0$ amplitudes are taken into account by viewing a meson decay as occurring via the breaking of the flux tube with the simultaneous creation of a quark-antiquark pair. To incorporate this into the $^3P_0$ model, the pair creation amplitude γ is allowed to vary in space so that the $q\bar{q}$ pair is produced within the confines of a flux-tube-like region surrounding the initial quark and antiquark. This model is described in detail in Ref. [8]. The $^3P_0$ model corresponds to the limit in which γ is constant.

For the $^3P_0$ model using simple harmonic oscillator wave functions, the S and D amplitudes are given by

$$S=\left[3-q^2\left(\frac{m_{13}\beta_B^2+m_{23}\beta_C^2}{3\beta_B^4\beta_C^4}\right)\right.$$
$$\left.\times[3\beta_B^2\beta_C^2-\beta^2(m_{13}\beta_B^2+m_{23}\beta_C^2)]\right]F(q^2)A, \quad (30)$$

$$D=q^2\left(\frac{m_{13}\beta_B^2+m_{23}\beta_C^2}{3\beta_B^4\beta_C^4}\right)[3\beta_B^2\beta_C^2-\beta^2(m_{13}\beta_B^2+m_{23}\beta_C^2)]$$
$$\times F(q^2)A, \quad (31)$$

where

$$F(q^2)=\exp\left[\frac{-q^2}{6}\left(\frac{\beta^2[(m_{13}-m_{23})^2\beta_A^2+m_{13}^2\beta_B^2+m_{23}^2\beta_C^2]}{\beta_A^2\beta_B^2\beta_C^2}\right)\right], \quad (32)$$

$$A=\frac{2i\gamma}{27\pi^{1/4}\beta^{1/2}}\left(\frac{\beta}{\beta_A}\right)^{5/2}\left(\frac{\beta^2}{\beta_B\beta_C}\right)^{3/2}q^{1/2}\left(\frac{\tilde{M}_B\tilde{M}_C}{\tilde{M}_A}\right)^{1/2}, \quad (33)$$

$$\beta^{-2}=\frac{1}{3}(\beta_A^{-2}+\beta_B^{-2}+\beta_C^{-2}), \quad (34)$$

$$m_{13}=\frac{m_1}{m_1+m_3}, \quad (35)$$

$$m_{23}=\frac{m_2}{m_2+m_3}, \quad (36)$$

m_1 and m_2 are the quark and antiquark masses from the original meson, m_3 is the mass of the created quark or antiquark, the β_i are the simple harmonic oscillator wave function parameters, and q is the momentum of each outgoing meson in the CM frame. For these results we take the $\tilde{M}_i$ to be equal to the calculated masses of the mesons in a spin-independent potential [8]. Numerical values for the relevant amplitudes are given in Table III.

The decay amplitudes in the $^3P_0$ model were computed symbolically using MATHEMATICA [25]. In the flux-tube-breaking model, two of the six integrals were done analytically; the remaining four were done numerically. The integrands were prepared symbolically using MATHEMATICA and then integrated numerically using either adaptive Monte Carlo (VEGAS [26]) or a combination of adaptive Gaussian quadrature routines.

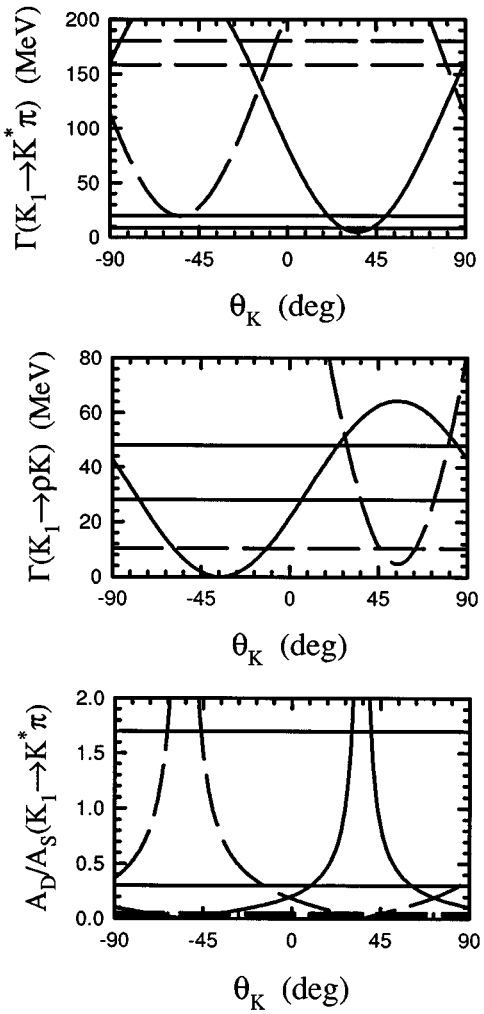

FIG. 3. Predictions of the pseudoscalar emission model as functions of θ_K for the K_1 partial widths (to $K^*\pi$ and ρK), and ratio of D to S amplitudes (to $K^*\pi$). The solid curves are for the $K_1(1270)$ and the dashed curves are for the $K_1(1400)$. The horizontal lines are the $1-\sigma$ error bounds for the experimental measurements [21] with the same line labelling (solid, dashed) as the predictions. [The experimental lower bound for $K_1(1400)\rightarrow\rho K$ lies on the axis.]

We calculated the K_1 strong decays using both the flux-tube-breaking model, and the $^3P_0$ model for several sets of wave functions. In all cases we fitted γ to 28 of the best-known meson decays by minimizing the χ^2 defined by $\chi^2=\Sigma_i(\Gamma_i^{\text{theory}}-\Gamma_i^{\text{expt}})^2/\delta\Gamma_i^2$ where $\delta\Gamma_i$ is the experimental error.[4] The details of these fits are given in Ref. [27]. We performed a second fit to the K_1 decays where we allowed both θ_K and γ to vary. The value of θ_K obtained in the second approach did not change much from the first value, the main difference being that the χ^2 in the second fit was reduced substantially. The values for γ obtained in the second set of fits are consistent, within errors, with those obtained by the global fit of Ref. [27]. In Fig. 4 we show the

[4]For the calculations in the flux-tube-breaking model, a 1% error due to the numerical integration was added in quadrature with the experimental error.

TABLE IV. Partial decay widths and ratios of D to S amplitudes of the strange axial mesons for the pseudoscalar emission model, the $^3P_0$ decay model and the flux-tube-breaking model using the fitted value of θ_K. The widths are given in MeV. A_D/A_S refers to the ratio of D to S amplitudes. The errors on θ_K are $1-\sigma$.

Decay	Experiment (Ref. [21])	Pseudoscalar emission	$^3P_0$ Set 1[b]	Flux-tube breaking[a] Set 1[b]	Set 2[c]
θ_K		48°±5°	45°±4°	44°±4°	51°±3°
$\Gamma(K_1(1270)\to\rho K)$	38±10	63	75	70	121
$\Gamma(K_1(1270)\to K^*\pi)$	14.4±5.5	16	12	11	35
$\lvert A_D/A_S(K_1(1270)\to K^*\pi)\rvert$	1.0±0.7	0.64	0.89	1.02	0.40
$\Gamma(K_1(1400)\to\rho K)$	5.2±5.2	7.9	12	13	6.7
$\Gamma(K_1(1400)\to K^*\pi)$	164±16	286	221	197	400
$\Gamma(K_1(1400)\to K\omega)$	1.7±1.7	2.3	3.6	3.9	1.9
$\lvert A_D/A_S(K_1(1400)\to K^*\pi)\rvert$	0.04±0.01	0.058	0.052	0.051	0.062

[a]Note that because the flux-tube-breaking calculation involves a numerical integral with a 1% error, the two values of S (or D) calculated from the $K_1(1270)$ and $K_1(1400)$ decay results may not agree exactly. In Table III an average value of the two results is given. Because the S and D values in Table III are not exact, using them with Eq. (26) will not exactly reproduce the flux-tube-breaking results show in this table, which are calculated directly from the numerical work.

[b]Simple harmonic oscillator wave functions with $\beta=0.40$ GeV, $m_u=0.33$ GeV, and $m_s=0.55$ GeV.

[c]Wave functions from Ref. [6].

decay widths and ratios of D to S amplitudes as functions of θ_K for the $^3P_0$ model. The results for the two variations of the flux-tube-breaking model are very similar and are therefore not shown. It is clear from these figures that θ_K will be approximately equal to 45°. The fitted values of θ_K for the various models, and the resulting widths, are given in Table IV.

V. DISCUSSION

One of the motivations for this analysis is to relate hadron properties to the underlying theory via *effective* interquark interactions [28]. We begin our discussion of the K_1 mesons by rewriting the nonrelativistic, spin-dependent potential in a more suitable form and interpreting it as an *effective* interaction [28]. We will later examine the K_1 meson properties in the limit $m_Q\to\infty$.

The spin-orbit Hamiltonian can be rewritten as

$$H_{q\bar{q}}^{\mathrm{SO(CM)}}=\frac{2}{3}\frac{\alpha_s}{r^3}\left(\frac{1}{m_q}+\frac{1}{m_{\bar{q}}}\right)^2\vec{S}\cdot\vec{L}+\frac{2}{3}\frac{\alpha_s}{r^3}\left(\frac{1}{m_q^2}-\frac{1}{m_{\bar{q}}^2}\right)\vec{S}_-\cdot\vec{L}, \tag{37}$$

$$H_{q\bar{q}}^{\mathrm{SO(TP)}}=-\frac{1}{4r}\frac{\partial H_{q\bar{q}}^{\mathrm{conf}}}{\partial r}\left[\left(\frac{1}{m_q^2}+\frac{1}{m_{\bar{q}}^2}\right)\vec{S}\cdot\vec{L}+\left(\frac{1}{m_q^2}-\frac{1}{m_{\bar{q}}^2}\right)\vec{S}_-\cdot\vec{L}\right], \tag{38}$$

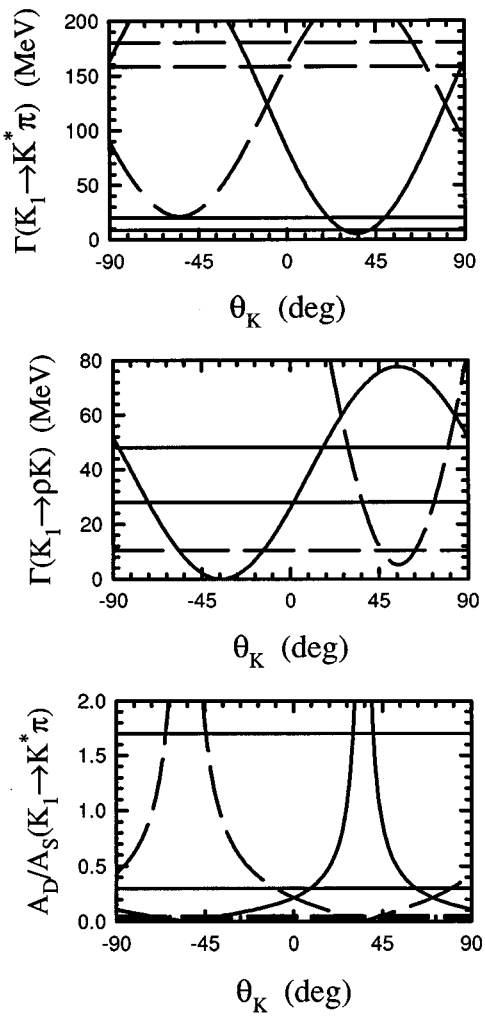

FIG. 4. Predictions of the $^3P_0$ model as functions of θ_K for the K_1 partial widths (to $K^*\pi$ and ρK), and ratio of D to S amplitudes (to $K^*\pi$). The line labeling is the same as in Fig. 3.

where $\vec{S}=\vec{S}_q+\vec{S}_{\bar{q}}$, $\vec{S}_-=\vec{S}_q-\vec{S}_{\bar{q}}$. Taking $\bar{q}=Q$, the various terms in $H^{\rm SO}$ can be rearranged as

$$H^{\rm SO}=H^+_{\rm SO}\vec{S}\cdot\vec{L}+H^-_{\rm SO}\vec{S}_-\cdot\vec{L}=H^q_{\rm SO}\vec{S}_q\cdot\vec{L}+H^Q_{\rm SO}\vec{S}_Q\cdot\vec{L}, \tag{39}$$

where the definitions of $H^+_{\rm SO}$, $H^-_{\rm SO}$, $H^q_{\rm SO}$, and $H^Q_{\rm SO}$ follow from Eqs. (37) and (38). It is the $H^-_{\rm SO}$ term which gives rise to the spin-orbit mixing between the singlet and triplet states. With this Hamiltonian, we obtain the mass formulas for the P-wave mesons

$$M(^3P_2)=M_0+\frac{1}{4}\langle H_{\rm cont}\rangle-\frac{1}{10}\langle H_{\rm ten}\rangle+\langle H^+_{\rm SO}\rangle,$$

$$\begin{pmatrix} M(^3P_1)\\ M(^1P_1)\end{pmatrix}=\begin{pmatrix} M_0+\frac{1}{4}\langle H_{\rm cont}\rangle+\frac{1}{2}\langle H_{\rm ten}\rangle-\langle H^+_{\rm SO}\rangle & \sqrt{2}\langle H^-_{\rm SO}\rangle\\ \sqrt{2}\langle H^-_{\rm SO}\rangle & M_0-\frac{3}{4}\langle H_{\rm cont}\rangle\end{pmatrix}\begin{pmatrix} ^3P_1\\ ^1P_1\end{pmatrix},$$

$$M(^3P_0)=M_0+\frac{1}{4}\langle H_{\rm cont}\rangle-\langle H_{\rm ten}\rangle-2\langle H^+_{\rm SO}\rangle, \tag{40}$$

where the $\langle H_i\rangle$ are the expectation values of the spatial parts of the various terms, M_0 is the center of mass of the multiplet, and we have adopted a phase convention corresponding to the order of coupling $\vec{L}\times\vec{S}_q\times\vec{S}_Q$.

We can rewrite $H^{\rm SO}$ using the substitutions $\overline{m}=\frac{1}{2}(m_q+m_Q)$ and $\Delta=(m_Q-m_q)$ to obtain the approximate expression

$$H^{\rm SO}\simeq\left[\frac{8}{3}\frac{\alpha_s}{\overline{m}^2r^3}-\frac{1}{2\overline{m}^2}\frac{1}{r}\frac{\partial H^{\rm conf}_{q\bar{q}}}{\partial r}\vec{S}\cdot\vec{L}\right.$$
$$\left.-\frac{\Delta}{\overline{m}}\left[\frac{4}{3}\frac{\alpha_s}{\overline{m}^2r^3}-\frac{1}{2\overline{m}^2}\frac{1}{r}\frac{\partial H^{\rm conf}_{q\bar{q}}}{\partial r}\right]\vec{S}_-\cdot\vec{L}. \tag{41}$$

Written in this way, one sees that there is a factor of 2 difference between the color magnetic term and the Thomas precession term for the $H^-_{\rm SO}$ relative to $H^+_{\rm SO}$. The observed spin-orbit splittings in hadrons indicate a delicate cancellation between the color magnetic and Thomas precession spin-orbit terms. Given this cancellation, the factor of 2 could lead to a large effect or even a sign reversal in the spin-orbit mixing.

In particular, the relativized quark model gives $\theta_K=-5°$ [3]. This originates from $\langle H^-_{\rm SO}\rangle\sim-1$ MeV. On the other hand, the various phenomenological measurements give $\theta_K\sim40°$ which implies a value of $\langle H^-_{\rm SO}\rangle\sim40$ MeV. Comparing these numbers to $\langle H^+_{\rm SO}\rangle\sim47$ MeV, extracted from Ref. [3], one can see that by extracting a value for $\langle H^-_{\rm SO}\rangle$ from θ_K and comparing it to the value for $\langle H^+_{\rm SO}\rangle$, one can obtain information about the relative strengths of the Coulomb and confining pieces of $H^{\rm conf}_{q\bar{q}}$. Given the sensitivity of the mixing angle to the delicate cancellation between terms, L-S mixing can therefore be a useful means of probing the confinement potential.[5]

We next consider the heavy quark limit, where $m_Q\to\infty$. In this limit the mass formulas simplify to

$$M(^3P_2)=M_0+\langle H^q_{\rm SO}\rangle,$$

$$\begin{pmatrix} M(^3P_1)\\ M(^1P_1)\end{pmatrix}=\begin{pmatrix} M_0-\langle H^q_{\rm SO}\rangle & \sqrt{2}\langle H^q_{\rm SO}\rangle\\ \sqrt{2}\langle H^q_{\rm SO}\rangle & M_0\end{pmatrix}\begin{pmatrix} ^3P_1\\ ^1P_1\end{pmatrix},$$

$$M(^3P_0)=M_0-2\langle H^q_{\rm SO}\rangle. \tag{42}$$

The two mixed K_1 mass eigenstates of $J^P=1^+$ appropriate to the heavy quark limit are described by the total angular momenta j of the light quark with $j=1/2$ and $j=3/2$ which are degenerate with the $J^P=0^+$ and $J^P=2^+$ states, respectively. In what follows, we will take $\langle H^q_{\rm SO}\rangle$ positive but similar results are obtained for $\langle H^q_{\rm SO}\rangle$ negative. For $\langle H^q_{\rm SO}\rangle>0$, the mixing angle is given by $\sin\theta_K=-\sqrt{2/3}$ and $\cos\theta_K=\sqrt{1/3}$ ($\theta_K=-54.7°$) with $M_{K_{\rm low}}$ degenerate with the $^3P_0$ ($j=1/2$) state and $M_{K_{\rm high}}$ degenerate with the $^3P_2$ ($j=3/2$) state.

For the K_1 decay constants, in the limit that $m_{\bar{s}}$ becomes infinitely heavy, the f_{K_1} become proportional to the inverse of the light quark mass and are given by

$$f_{K_{\rm low}}=\frac{\sqrt{3}A}{m_u},\quad f_{K_{\rm high}}=0. \tag{43}$$

So, in the heavy quark limit, only the $j=1/2$ state couples to the weak current. By comparing this result to the measured

[5]Nevertheless, one cannot rule out the possibility that another mechanism is responsible for $^3P_1$-$^1P_1$ mixing such as mixing via common decay channels [29].

decays, one might learn how well the heavy quark limit describes the strange axial mesons. Using the value of θ_K that gives the $j=1/2$ and $j=3/2$ eigenstates (expected in the heavy quark limit) and using a finite mass strange quark (still taking $\langle H^q_{\rm SO}\rangle > 0$), the decay constants are given by

$$f_K(j=1/2) = +\frac{\sqrt{3}A}{m_u}\left(1+\frac{m_u}{3m_s}\right),$$
$$f_K(j=3/2) = -\sqrt{\frac{8}{3}}\frac{A}{m_s}. \tag{44}$$

The value does not change very much for the $j=1/2$ state, $m_u/3m_s \simeq 0.2$, but the $j=3/2$ state decay constant is no longer zero; rather it is now similar in magnitude to that of the $j=1/2$ state.

More importantly, the θ_K we used in the above discussion was based on the $J^P=1^+$ mass matrix obtained for the heavy quark limit which assumes that the contact and tensor contributions are negligible. However, values for these terms extracted from predictions of the relativized quark model [3] are: $\langle H_{\rm cont}\rangle = 33$ MeV, $\langle H_{\rm ten}\rangle = 56$ MeV, and $\langle H^+_{\rm SO}\rangle = 47$ MeV. Clearly, the assumption that the contact and tensor pieces are negligible is not supported by this model so that the heavy quark limit is questionable for the s quark.

We conclude that while the heavy quark limit is an interesting means of making qualitative observations, the actual situation for the strange axial mesons is far more complicated.

VI. CONCLUSIONS

In this paper we studied the properties of the strange axial mesons in the quark model. We extracted the $K_1(^3P_1)$-$K_1(^1P_1)$ mixing using the mass predictions, by comparing a quark model calculation of the K_1 decay constants to the decays $\tau \to \nu_\tau K_1$, and by comparing strong decay widths calculated using the pseudoscalar emission model and the flux-tube-breaking model to experimental results. In all cases we obtained a mixing angle consistent with $\theta_K \simeq 45°$. There are two important conclusions we can draw from this result. First, the relativized quark model predicts a much smaller mixing angle of $\sim -5°$. Either the quark model result is way off, which is possible given the delicate cancellation taking place between the contributions to the spin-orbit term, or a different mechanism is responsible for the $^3P_1$-$^1P_1$ mixing [29]. The second observation we make on the basis of the quark model results is that the heavy quark limit does not appear to be applicable to the strange axial mesons. We come to this conclusion because the tensor interaction is still comparable in size to the spin-orbit interactions and additionally, the mixing angle is not compatible with that expected in the heavy quark limit.

ACKNOWLEDGMENTS

This research was supported in part by the Natural Sciences and Engineering Research Council of Canada. The authors thank Sherry Towers for discussion and S.G. thanks Nathan Isgur for helpful conversations.

[1] A. De Rújula, H. Georgi, and S.L. Glashow, Phys. Rev. Lett. **37**, 785 (1976).
[2] J. Rosner, Comments Nucl. Part. Phys. **16**, 109 (1986).
[3] S. Godfrey and R. Kokoski, Phys. Rev. D **43**, 1679 (1991).
[4] TPC/Two-Gamma Collaboration, D.A. Bauer *et al.*, Phys. Rev. D **50**, R13 (1994).
[5] S. Towers (private communication).
[6] S. Godfrey and N. Isgur, Phys. Rev. D **32**, 189 (1985).
[7] S. Godfrey, Phys. Rev. D **31**, 2375 (1985); S. Godfrey and N. Isgur, *ibid.* **34**, 899 (1986).
[8] R. Kokoski and N. Isgur, Phys. Rev. D **35**, 907 (1987); see also P. Geiger and E.S. Swanson, *ibid.* **50**, 6855 (1994) for further calculational details.
[9] M. Suzuki, Phys. Rev. D **47**, 1252 (1993).
[10] M. Suzuki, Phys. Rev. D **50**, 4708 (1994).
[11] D. Gromes, in *The Quark Structure of Matter*, Proceedings of the Yukon Advanced Study Institute, edited by N. Isgur, G. Karl, and P.J. O'Donnell (World Scientific, Singapore, 1985).
[12] E.W. Colglazier and J.L. Rosner, Nucl. Phys. **B27**, 349 (1971); H.J. Lipkin, Phys. Lett. **72B**, 249 (1977).
[13] S. Capstick and S. Godfrey, Phys. Rev. D **41**, 2856 (1990).
[14] A. La Yaouanc, L. Oliver, O. Pène, and J.-C. Raynal, Phys. Rev. D **9**, 2636 (1974); M.J. Ruiz, *ibid.* **12**, 2922 (1975).
[15] C. Hayne and N. Isgur, Phys. Rev. D **25**, 1944 (1982).
[16] S. Godfrey, Phys. Rev. D **33**, 1391 (1986).
[17] N. Isgur, D. Scora, B. Grinstein, and M.B. Wise, Phys. Rev. D **39**, 799 (1989).
[18] P. Colić, B. Guberina, D. Tadić, and J. Trampetić, Nucl. Phys. **B221**, 141 (1983); J. Trampetić, Phys. Rev. D **27**, 1565 (1983).
[19] R. Alemany, in *Proceedings of the XXVII International Conference on High Energy Physics*, Glasgow, Scotland, 1994, edited by P.J. Bussey and I.G. Knowles (Institute of Physics Publishing, Bristol, 1995), p. 1081.
[20] CLEO Collaboration, M. Athanas *et al.*, in *Proceedings of the XXVII International Conference on High Energy Physics* [19]; B.K. Heltsley, in *Tau 94*, Proceedings of the *Third Workshop on Tau Lepton Physics*, Montreux, Switzerland, 1994, edited by L. Rolandi [Nucl. Phys. B (Proc. Suppl.) **40**, 413 (1995)]; see also the recent ARGUS result, ARGUS Collaboration, H. Albrecht *et al.*, Z. Phys. C **68**, 215 (1995).
[21] Particle Data Group, L. Montanet *et al.*, Phys. Rev. D **50**, 1173 (1994).
[22] The spin-dependent terms arise from a (v/c) expansion of the two fermion scattering amplitude via one-gluon exchange. See, for example, V.B. Berestetskii, E.M. Lifshitz, and L.P. Pitaevskii, *Quantum Electrodynamics*, 2nd ed. (Pergamon, Oxford, 1982), p. 336.
[23] R.K. Carnegie *et al.*, Phys. Lett. **68B**, 287 (1977); H.J. Lipkin, Phys. Rev. **176**, 1709 (1968), and references therein.
[24] A. Le Yaouanc, L. Oliver, O. Pène, and J.-C. Raynal, Phys.

Rev. D **8**, 2223 (1973); **9**, 1415 (1974); **11**, 1272 (1975); M. Chaichian and R. Kögerler, Ann. Phys. (N.Y.) **124**, 61 (1980); W. Roberts and B. Silvestre-Brac, Few-Body Systems **11**, 171 (1992).

[25] Stephen Wolfram, ‘‘ MATHEMATICA: A SYSTEM FOR DOING MATHEMATICS BY COMPUTER,’’ 2nd ed. (Addison-Wesley, Redwood City, CA, 1991); for the flux-tube-breaking model of meson decay, FORTRAN code was created using the MATHEMATICA packages Format.m and Optimize.m, written by M. Sofroniou and available from MathSource (URL: http://www.wri.com/).

[26] G. Peter Lepage, J. Comput. Phys. **27**, 192 (1978); ‘‘VEGAS—An Adaptive Multi-dimensional Integration Program,’’ Cornell University Technical Note CLNS-80/447, 1980.

[27] H.G. Blundell and S. Godfrey, this issue, Phys. Rev. D **53**, 3700 (1996).

[28] For some discussion and applications of this approach see H. Schnitzer, Phys. Lett. B **226**, 171 (1989); S. Godfrey, Phys. Lett. **162B**, 367 (1985); H. Schnitzer, *ibid*. **134B**, 2153 (1984); **149B**, 408 (1984); Nucl. Phys. **B207**, 131 (1983).

[29] H.J. Lipkin, Phys. Lett. **72B**, 249 (1977).